Ultrastructural Pathology

ISSN: 0191-3123 (Print) 1521-0758 (Online) Journal homepage: http://www.tandfonline.com/loi/iusp20

Spotlight on the three main hepatic fibrogenic cells in HCV-infected patients: Multiple immunofluorescence and ultrastructure study

Soheir S. Mansy PhD, Mona M. Nosseir MD, May M. Othman MSc, Mona A. Zoheiry MD, Mohammed F. Guda MD, Hoda A. Yehia PhD & Moataz H. Hassanein MD

To cite this article: Soheir S. Mansy PhD, Mona M. Nosseir MD, May M. Othman MSc, Mona A. Zoheiry MD, Mohammed F. Guda MD, Hoda A. Yehia PhD & Moataz H. Hassanein MD (2016): Spotlight on the three main hepatic fibrogenic cells in HCV-infected patients: Multiple immunofluorescence and ultrastructure study, Ultrastructural Pathology, DOI: 10.1080/01913123.2016.1194507

To link to this article: http://dx.doi.org/10.1080/01913123.2016.1194507

Published online: 13 Jul 2016.

ULTRASTRUCTURAL PATHOLOGY
http://dx.doi.org/10.1080/01913123.2016.1194507

Taylor & Francis
Taylor & Francis Group

ORIGINAL ARTICLE

Spotlight on the three main hepatic fibrogenic cells in HCV-infected patients: Multiple immunofluorescence and ultrastructure study

Soheir S. Mansy, PhD[a], Mona M. Nosseir, MD[b], May M. Othman, MSc[a], Mona A. Zoheiry, MD[c], Mohammed F. Guda, MD[d], Hoda A. Yehia, PhD[a], and Moataz H. Hassanein, MD[d]

[a]Electron Microscopy Research Department (Pathology), Theodor Bilharz Research Institute, Giza, Egypt; [b]Pathology Department, Theodor Bilharz Research Institute, Giza, Egypt; [c]Immunology Department, Theodor Bilharz Research Institute, Giza, Egypt; [d]Hepatogastroenterology Department, Theodor Bilharz Research Institute, Giza, Egypt

ABSTRACT

The present work deals with the simultaneous ultrastructure and triple immunofluorescence study of the three main hepatic fibrogenic cells, hepatic stellate cell, myofibroblast (MF), and fibroblast, in a group of hepatitis C virus (HCV) RNA positive patients, as their exact interrelation behavior in vivo with the progress of hepatic fibrosis is still inadequate. In this study, for the first time, cells having the morphological characteristic of MF and not bone marrow fibrocytes were revealed in liver portal vessels. This necessitates the reevaluation of the available knowledge concerning bone marrow fibrocyte. Also, the distribution, cellular interrelations, and the fate of MF were highlighted.

ARTICLE HISTORY
Received 13 May 2016
Accepted 23 May 2016
Published online 14 July 2016

KEYWORDS
Bone marrow fibrocyte; fibroblast; hepatic stellate cell; liver fibrosis; myofibroblast

Introduction

Hepatitis C virus (HCV) infection is one of the major causes of chronic liver disease worldwide. The number of chronically infected persons is approximately about 160–185 million persons [1,2]. Fibrosis and cirrhosis with or without hepatocellular carcinoma (HCC) are the main long-term impact of HCV and the main causes of morbidity and mortality [2,3]. The currently available management is liver transplantation. Thus, the need for organs is continually increasing and many patients die while being on the waiting list [4]. On the other hand, an important alternative is the modulation of the fibrogenic process by better understanding of the contributing factors and the development of antifibrotics. Until now, despite the running researches no effective drugs have been validated in the clinical practice [5,6].

Hepatic stellate cells, myofibroblasts, and portal fibroblasts have been shown to be crucial players in the process of hepatic fibrogenesis [7–15]. Many researchers have tackled these cells from diverse aspects as morphological, molecular, functional, and secreted material [13,14,16–21]. Also, Nepomnyashchikh et al. [22] and Mansy et al. [23] have shed light on hepatic stellate cells in patients with HCV at an ultrastructure level. Meanwhile, the exact behavior of these cells is still inadequate and the origin of myofibroblasts is not yet resolved [13,24]. As well as, to our knowledge, no one has laid importance to the dynamic and interrelation of these cells in vivo with the progress of hepatic fibrosis.

The aim of this study is to determine the overall impact value of these cells on the process of hepatic fibrogenesis. This is achieved not solely based on the available specific markers of these cells using triple immunofluorescence technique but also on their morphology and interaction at an ultrastructure level. Moreover, correlation of the quantitative assessment of these cells with the corresponding evaluation of serum levels of hyaluronic acid and morphometric image analysis of collagen in liver sections is considered. Serum hyaluronic acid is among the most validated non-invasive serum biomarkers for monitoring hepatic fibrosis [25,26]. Meanwhile, this study has

CONTACT Soheir S. Mansy soher.mansy@live.com; s.mansy@tbri.gov.eg Electron Microscopy Research Department (Pathology), Theodor Bilharz Research Institute, El Nile Street, Warrak-El Hadar, Imbaba 12411, Giza, Egypt.

Color versions of one or more of the figures in this article can be found online at www.tandfonline.com/iusp.

used fibroblast surface proteins, α smooth muscle actin and reelin, which are secreted by fibroblast cells, myofibroblasts, and HSC, respectively, as specific markers for the determination of these cells in the same immunostained liver section [17,27–31]. The prospective of this work is to increase our understanding of the available knowledge and to point out the cells that deserve to be inactivated to control the progress of fibrosis.

Material and methods

A total of 64 cases positive for serum HCV RNA confirmed by polymerase chain reaction and having HCV genotype 4 were enrolled in this study. They all were above 19 years of age. They were among the patients admitted consecutively to Theodor Bilharz Research Institute at the hepatogastroenterology department for performing liver biopsy or acquiring treatment between 2013 and 2014. All the patients subjected to this study had not any additional cause of chronic liver diseases as result of other viral infections, parasitic infections, and biliary or metabolic disorders. They were not subjected to antifibrotic, immunosuppressive, or antiviral treatment. They did not have any associated organic diseases such as osteoarthritis, autoimmune diseases, rheumatoid arthritis, or HCC. These patient's inclusion and exclusion criteria were determined after complete clinical examination and laboratory investigations.

A control group consisting of 15 age-matched healthy volunteers was involved in the study. They were subjected only to blood sample collection for the assessment of serum hyaluronic acid.

This study was approved by Theodor Bilharz Research Institute Institutional Review Board. Informed consent was taken from all patients according to the rules of Declaration of Helsinki before any medical intervention.

Samples collection and processing

Two percutaneous liver core biopsies were taken from each patient by applying Menghini's technique. Hepafix needle with 16 gauge was used under ultrasound guidance. Fasting blood sample (3 ml) was collected from the patients and the control group for the analysis of serum hyaluronic acid.

The harvested liver biopsies were processed for:

Electron microscopic examination

One core of liver specimens was divided into tiny pieces of about 1 mm^3 and fixed in 4% buffered glutaraldehyde (SERVA, Frankfurt, Germany) in 0.2% cacodylate (TAAB essential for microscopy, Aldermaston, Berks, UK) and processed for electron microscopic examination. The fixed liver biopsies were washed in equal volumes of 0.3 M cacodylate and sucrose 0.4 M for two successive baths of 1 h each, then postfixed in 2% osmium tetroxide (TAAB essential for microscopy, Aldermaston, Berks, England) for 2 h, dehydrated in ascending concentrations of alcohol and propylene oxide and embedded in epoxy resin. Inclusion in gelatin capsules was performed using the mixture of Epon 812, dodecenyl succinic anhydride, methyl nadic anhydride, and benzyldimethylamine (Electron Microscopy Sciences, Hatfield, PA). Polymerization was done at 60°C for 48 h. Semithin liver sections of 1 µm thick were performed using the ultramicrotome (Leica Ultracut R, Vienna, Austria). The sections were stained with methylene blue and azur II for the selection of the sites to perform ultrathin sections. The midzonal and periportal areas of hepatic lobule as well as the portal tract were the considered sites. Ultrathin liver sections were done. They were stained with uranyl acetate 7% in water and lead citrate (Loba Chemie Pvt. Ltd., Colaba, Mumbai, India). The differentiation between the three studied fibrogenic cells at the ultrastructure level was based on the previously reported morphologic criteria of each cell [32]. Ultrastructure examination of the ultrathin liver sections was done using Phillips Electron Microscope 208S (FEI Company, Eindhoven, The Netherlands).

Formation of paraffin block for light and confocal laser scanning microscopic examination

The second core of liver biopsies not less than 2.5 cm in length was fixed in 10% buffered formalin and processed until embedded in paraffin blocks for light and confocal laser scanning microscopic procedures.

Histological examination of liver samples. Serial liver sections of 4 µm thickness were performed from the paraffin-embedded liver biopsies. They were stained with hematoxylin and eosin and Masson Trichrome. The stage of fibrosis and necroinflammatory grade of activity were assessed according to the METAVIR scoring

system [33]. Fibrosis was staged on a scale of 0–4 in which F4 constitutes liver cirrhosis. It was further grouped into moderate fibrosis (F1 + F2) and severe hepatic fibrosis (F3 + F4) [34–36].

Morphometric image analysis of hepatic collagen. Liver sections of 5 μm thickness were stained with Sirius red. Fibrous tissue appeared pink in a colorless background. Morphometric measurement was carried out using the Kontron image analysis system with the Rel.4.8 Axio Vision software program. The pink-colored stained collagen with Sirius red was measured in the sections as a percentage of quantifiable, integrated, optical density (IOD) of the sum of the area of microscopic fields. For each patient, five fields per slide illustrating maximum area of fibrosis were evaluated using 5× Zeiss objective lens and the mean value was considered.

Triple immunofluorescence staining of the three studied cells. The technique was applied to identify and assess the three studied fibrogenic cells: HSC, myofibroblast, and fibroblast in the same liver section.

The triple immunofluorescence technique using multiple fluorochromes was performed on 5 μm thick deparaffinized liver sections deposited on Super Frost Plus glass slides [37]. The applied primary antibodies were mouse anti-human reelin antibody (Santa Cruz Biotechnology, Inc., Dallas, TX) for the determination of hepatic stellate cells; rabbit anti-human fibroblast surface protein 1B10 (FSP) (Biorbyt, Berkeley, CA) for the determination of fibroblast; and goat anti-human smooth muscle a-actin (Sigma-Aldrich, Darmstadt, Germany) for the determination of myofibroblast. A mixture of these primary antibodies was applied on the studied sections in the dilution of 1:150, 1:50, and 1:100, respectively. The secondary antibodies were donkey affinipure anti-goat IgG antibody cyanine (CY2) conjugated (Rockland Antibodies and Assays, Limerick, PA); donkey affinipure anti-mouse IgG antibody aminomethylcoumarin (AMCA) conjugated (Jackson ImmunoResearch Laboratories, West Grove, PA); and donkey affinipure anti-rabbit IgG antibody indocarbocyanine (CY3) conjugated (Jackson ImmunoResearch Laboratories). A mixture of labeled secondary antibodies in the dilution of 1:400, 1:150, and 1:200 were applied for the revelation of primary antibodies. The AMCA, the CY2, and the CY3 labels are visualized as blue, green, and red, respectively, when excited with laser wavelength. Dako EnVisiona FLEX Target retrieval solution, high pH (50×) (Dako Denmark A/S, Glostrup, Denmark) was used for epitope antigen retrieval according the manufacturer's manual for the reagent. The stained slides were mounted using ready-to-use Dako faramount aqueous mounting media. Negative control samples were processed concomitantly in the same run according to the standard protocols. The immunofluorescence stained slides were examined using confocal laser scanning microscope (Carl Zeiss 710, Zeiss International, Oberkochen, Germany). The used software was ZEN, 2009 version. The applied laser wavelengths were 405, 458, 488, 514, 543, and 633 nm. Examination was done using the objective: Plan-apochromat 63× oil, EC plan-neofluar 40× oil, 20×, and 10×. Scoring of the positively stained immunoreactive cells in five images showing maximum reaction was done, and the mean value was calculated for each patient's sample. The images were taken for each sample at the level of CLSM using EC plan, neofluar 40×/1.30 oil DIC M27.

Determination of serum hyaluronic acid with ELISA technique

Serum hyaluronic acid was assessed using the quantitative sandwich immunoassay technique. A commercially available enzyme-linked immunosorbent assay (ELISA) kit was applied. The microtiter plate has been pre-coated with a polyclonal HA antibody. The detection reagent was horseradish peroxidase (HRP)–conjugated polyclonal antibody for HA. The chromogenic substrate was A and B solution (BlueGene Biotech Co., Ltd., Shanghai, China). The manufacturer-reported sensitivity of the applied ELISA kit was 1.0 ng/ml, the intra-assay variability coefficient of variation (CV) was <10% and inter-assay CV was <12%.

The technique was achieved according the instructions in the manufacturer reagent's operation manual. Standards and samples were done at the same time. The measurement of the color change was done using the spectrophotometer at a wavelength of 450 nm (ELISA reader BioRad, Marnes-la-Coquette, France). The quantitative

measurement of serum hyaluronic acid in the samples was interpolated from the appropriate standard curve according to the OD of the samples. All assays were performed in duplicate.

Statistical analysis

Statistical analysis of data was done using Statistical Package for Social Sciences (SPSS), version 21. Numerical data were summarized using means and standard deviations. Data were explored for normality using Kolmogorov–Smirnov test and Shapiro–Wilk test. Exploration of data revealed that the collected values were not normally distributed. Comparisons between the two groups were done by Mann–Whitney test. Comparisons between more than two groups were performed using the Kruskal–Wallis nonparametric test. This test was followed by the post hoc Bonferroni corrections to adjust the *P*-values. Univariate analyses were performed to select a first set of features to be tested for inclusion in a multivariate model. All features with a *P*-value less than 0.1 were included in the stepwise logistic regression model. Estimated odds ratios (ORs) with confidence intervals (CIs) were calculated. To assess the degree of association between the different measurements, the Spearman's correlation coefficient was calculated. All *P*-values are two-sided. *P*-values <0.05 were considered significant.

Results

Examination of the three fibrogenic cells at the CLSM and EM levels

The distribution of HSCs, myofibroblasts, and fibroblasts in the studied liver sections stained with multiple fluorochromes was identified. Reelin immunoreactivity, which is the marker of HSCs, showed preferential intralobular localization in the intercellular and perisinusoidal areas. Scattered cells were detected in the portal tract and septal fibrosis, especially in stages F3 and F4 fibrosis. The green α smooth muscle actin immunoreactivity denoting stained myofibroblasts was mostly confined to the portal tract in stage F1 hepatic fibrosis. They revealed outspreading to the periportal and lobular areas in stages F2–F4. In these later stages, positive green myofibroblast processes were seen extending in the liver lobule along blood sinusoids and intercellular areas. The smooth muscle cells (SMCs) forming the wall of blood vessels showed equally intense green fluorescent reaction for α smooth muscle actin. These SMCs were not included in myofibroblast cellular count. Immunoreactivity for fibroblast surface protein was scarcely detected in the examined sections in comparison with the immunoreactivity of reelin and α smooth muscle actin. They were mainly restricted to portal tracts. Co-localization of red fibroblast surface protein immunoreactivity in α smooth muscle actin positive myofibroblasts was mostly seen in stage F4 fibrosis. The overlapped co-localized immunostaining took orange-yellow coloration. Also, co-localization of reelin and α smooth muscle actin positive myofibroblasts was often detected. They were clearly distinguished in the same cell. The co-localization of the three markers was not disclosed in the same cell in the examined sections (Figures 1 and 2).

This distribution of the three fibrogenic cells, seen at the level of the multiple fluorochromes stained sections, was similar to their location identified by electron microscopy (EM). Myofibroblast constituted the main cell detected in examined sections especially in stage F2 fibrosis upward to stage F4 fibrosis. The detected myofibroblasts in liver lobule were mainly of HSC origin. They were characterized by the presence of single intracytoplasmic fat droplet. Fibroblasts whenever detected were seen mainly in the vicinity of myofibroblasts. Fibroblast and myofibroblast cells were not noticed in the Disse space. Instead, thin cytoplasmic cellular spindle-shaped structures showing cytoplasmic fibrillary material were frequently depicted in the Disse space and intercellular areas. This cytoplasmic structure seems originating from myofibroblasts, as similar thin cellular projections extended from the myofibroblasts and appeared insinuating between the hepatocytes or communicating cells together were disclosed in the α smooth muscle actin immunostained sections. As well as, detached or cleaved cellular parts from myofibroblasts were visualized in the examined sections. Some of them showed bundles of cytoplasmic microfilaments. Myofibroblasts showing cleavage appeared mainly solitary and surrounded by fibrous tissue. Their rough endoplasmic reticulum was not hypertrophied. Their nuclei were

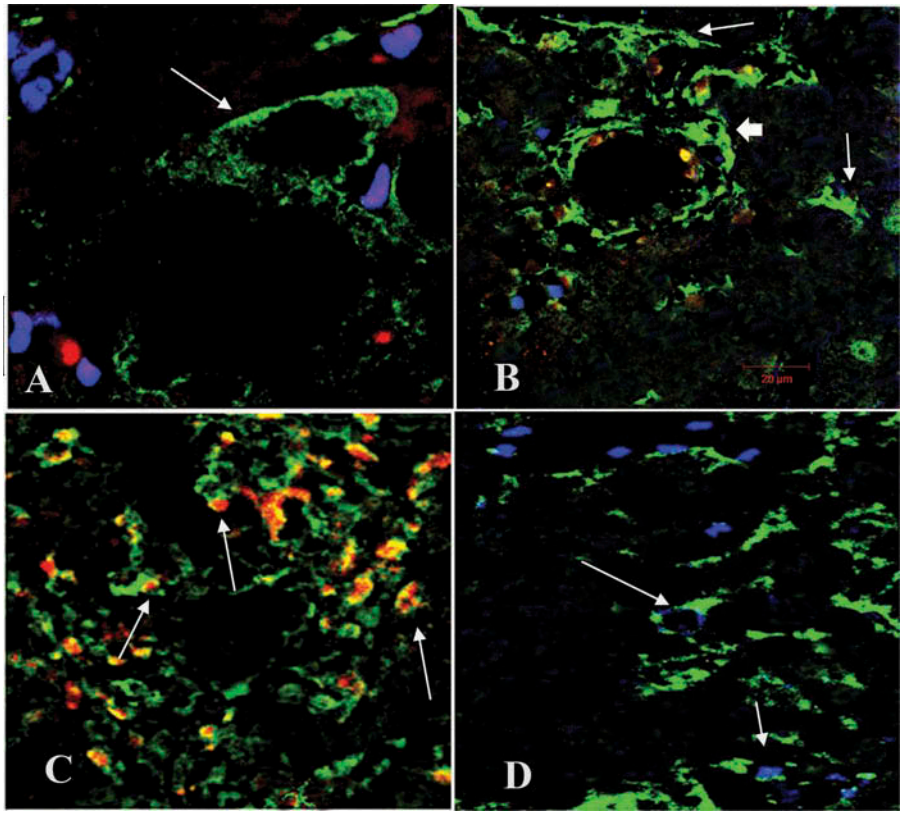

Figure 1. Triple fluorochromes stained liver sections using AMCA, CY2, and CY3 labels for reelin, α SMA, and FSP, respectively. (A) HSCs, fibroblasts, and myofibroblasts show blue, red, and green immunoreactivity, respectively. Note the extended cellular projections of myofibroblast (*arrow*). (B) Part of a portal tract shows positive myofibroblasts (*arrows*) and SMCs for α smooth muscle actin immunoreactivity. The latter takes circular configuration around blood vessels (*arrowhead*). (C) Co-localization of α smooth muscle actin and fibroblast surface protein in many cells (*arrows*). (D) Blue immunoreactivity for reelin in intimate localization with α smooth muscle actin of myofibroblasts (*arrows*) (40×/1.30 oil DIC M27 EC plan-neofluar).

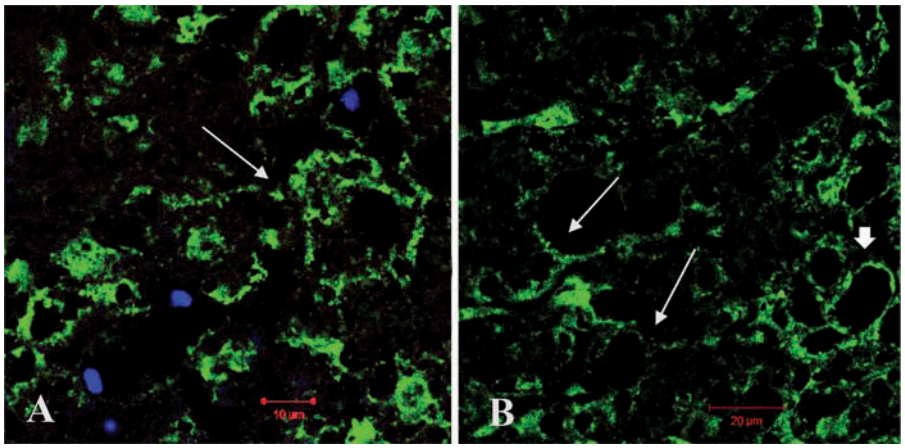

Figure 2. Triple immunofluorescence stained liver sections for the simultaneous visualization of HSCs, myofibroblasts (MF), and fibroblasts (Fb) cells. (A) Part of the liver lobule shows HSCs and myofibroblasts only. No fibroblasts are detected in the section. Myofibroblasts reveal extended cellular projections. (B) Myofibroblasts shows extending (*arrows*) and communicating cellular projections (*arrowhead*) (40×/1.30 oil DIC M27 EC plan-neofluar).

no more indented and the cells exhibited rudimentary basal lamina. They looked undergoing modulation to fibroblasts (Figure 3).

At the level of EM, spindle-shaped cells having the characteristic morphologic picture of myofibroblasts and not fibrocytes were depicted in the

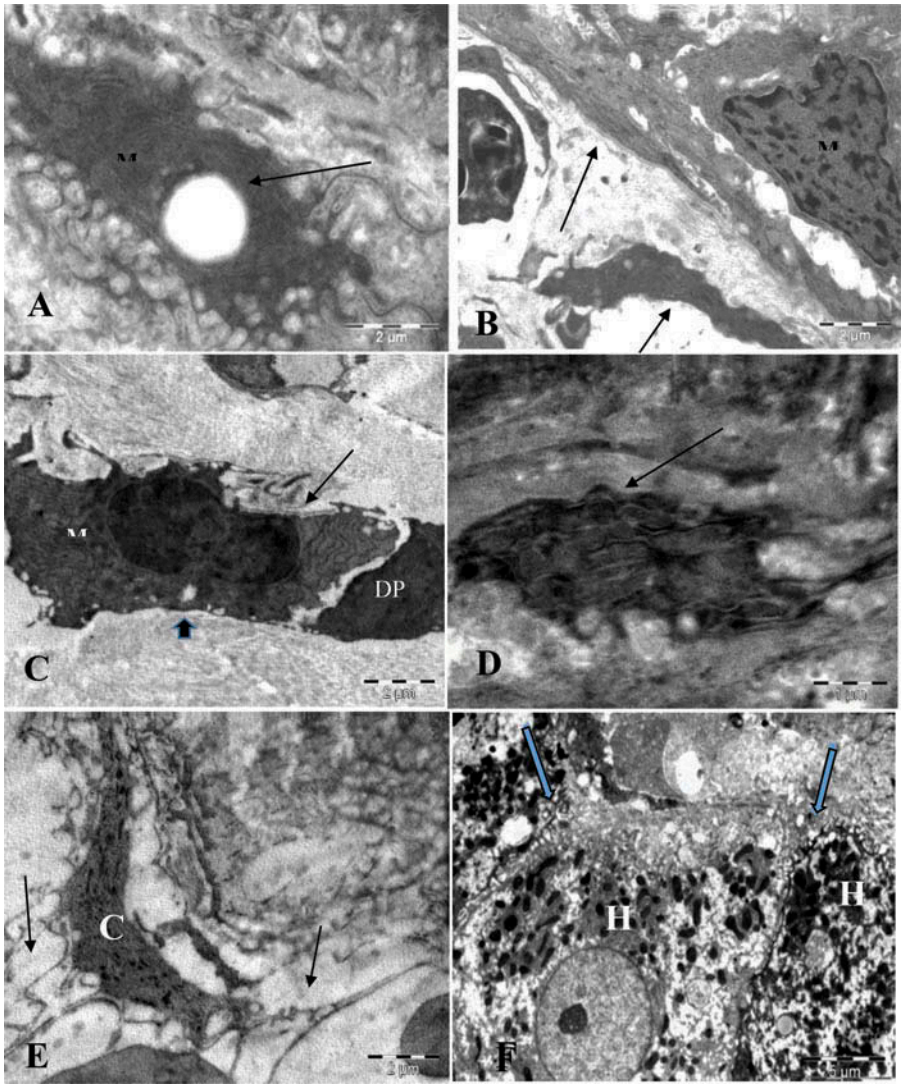

Figure 3. Electron micrographs showing different configurations of myofibroblasts, and their processes seen at the ultrastructure level. (A) Transdifferentiated myofibroblast (M) from HSC showing intracytoplasmic single fat droplet (*arrow*) and cellular cytoplasmic processes. (B) Myofibroblasts (M) and myofibroblast cellular projections (*arrows*). Note the rich rough endoplasmic reticulum, the cytoplasmic microfilament parallel to the long axis, dense bands, indented nucleus, dispersed nuclear chromatin, and partial basal lamina. (C) Myofibroblast (M) entangled by fibrous tissue undergoing modulation. It reveals quiescent rough endoplasmic reticulum, loss of nuclear indentation, rudimentary basal lamina (*arrow*), detached cellular part (DP), and another part showing starting of cleavage (*arrowhead*). It looks as if it transdifferentiates to fibroblast. (D) Detached part (*arrow*) from myofibroblast showing bundles of cytoplasmic microfilaments arranged parallel to the long axis. (E) Spindle-shaped cytoplasmic projection (C) devoid of nucleus mimic the cytoplasmic projections seen in Figure 3B. Shows plasmalemmal attachment plaques, dense bands, cytoplasmic microfilaments, and many long cytoplasmic processes extended in between cells. (F) Cytoplasmic processes (*arrows*) extending between hepatocytes (H).

portal circulation of the examined liver sections. These cells were characterized by fusiform indented nucleus, the presence of many pinocytotic vesicles along the cell membrane, plasmalemmal attachment plaques, and well-developed hypertrophied rough endoplasmic reticulum. This last criterion differentiates these cells from SMCs (Figure 4).

Relations between the three fibrogenic cells, stages of hepatic fibrosis, and hepatic fibrogenic parameters

Quantitative assessment of the three fibrogenic cells was performed in the liver sections of the studied cases. The results were correlated with the corresponding necroinflammatory activities, the stage of hepatic fibrosis, the values of the

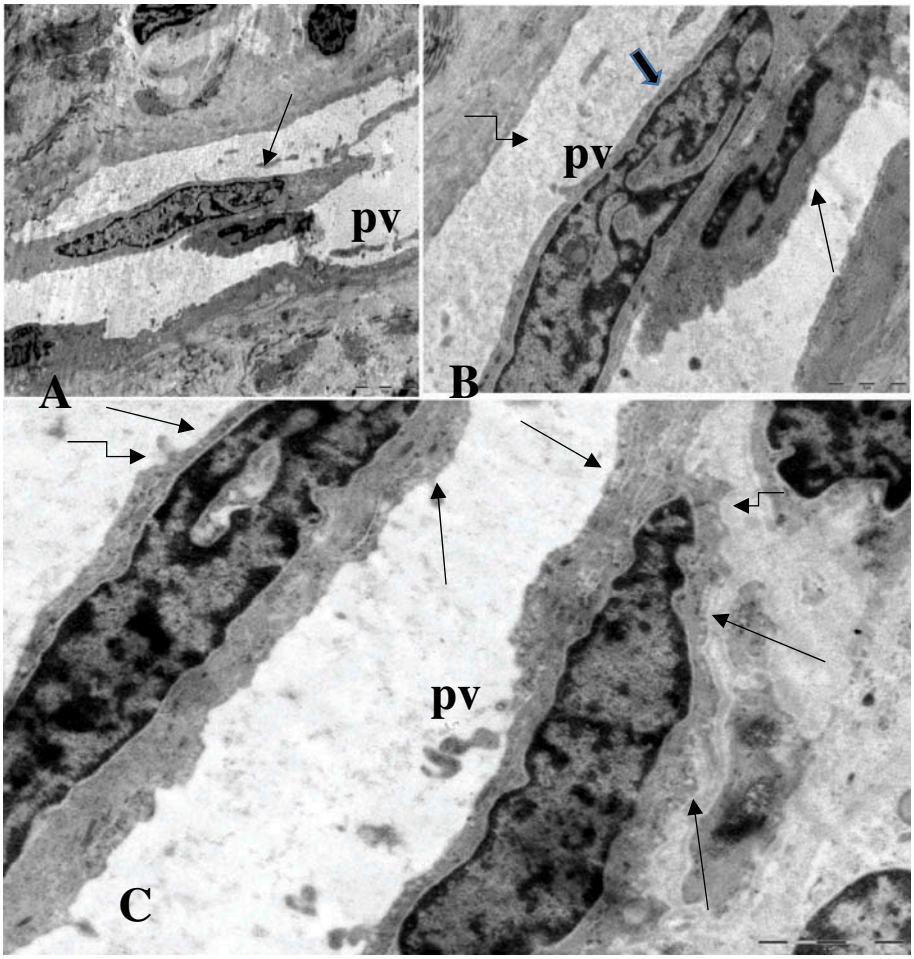

Figure 4. Electron micrograph showing myofibroblasts circulating in hepatic portal vein (P). (A) Two spindle-shaped cells with deep indented nucleus. (B and C) High power view of myofibroblasts circulating in the portal vein (P). They are spindle-like in shape. They show indented nucleus with dispersed chromatin, rich hypertrophied rough endoplasmic reticulum, pinocytotic vesicles (*arrows*), and fine cellular cytoplasmic projections (*bent arrows*).

morphometric quantitative assessment of fibrosis and the serum levels of HA (Tables 1–3, Figure 5).

The myofibroblasts showed significant increase in grade A3 activities versus grade A1 ($P < 0.012$). Meanwhile, the fibroblasts and HSCs did not reveal any relation with the degree of hepatic necroinflammatory activities. Moderate correlation was detected between the quantitative values of myofibroblast versus fibroblasts and hepatic stellate cells ($r = 0.461$, $P < .001$; $r = 0.489$, $P < .001$, respectively). Hepatic stellate cells revealed weak correlation with fibroblasts ($r = 0.254$, $P = .045$). Significant correlation was detected between the three cells and the morphometric image analysis of liver tissue collagen. This correlation was significantly moderate with the quantitative value of myofibroblasts ($r = 0.553$, $P < .001$) and weak with the other two cells. Good and moderate significant correlations were detected between the serum levels of HA

Table 1. Correlation between the grade of activity and the fibrogenic cells.

	Activity								
	0 ($n = 8$)		1 ($n = 30$)		2 ($n = 15$)		3 ($n = 11$)		
	Mean	Standard deviation	Mean	Standard deviation	Mean	Standard deviation	Mean	Standard deviation	*P*-value
Fb	9.3	3.7	8.3	3.5	10.0	2.9	8.9	3.0	.384
MF	24.5	6.7	23.1*	7.3	28.5	5.7	32.2*	7.9	.007
HSC	14.6	4.8	15.9	5.5	19.8	4.8	17.4	5.8	.066

P-values < .05 were considered significant.
*Significant.

Table 2. Correlation between the three fibrogenic cells and the morphometric image analysis of collagen, the stage of hepatic fibrosis, as well as serum hyaluronic acid.

	Spearman's ρ									
	HA (pg/ml)		MIA of collagen		Stage of fibrosis		Fb		MF	
	r	*P*-value	*r*	*P*-value	*r*	*P*-value	*r*	*P*-value	*r*	*P*-value
Fb	0.381#	.002	0.395#	.001	0.598^	< .001				
MF	0.660*	< .001	0.553^	< .001	0.750*	< .001	0.461^	< .001		
HSC	0.598^	< .001	0.260#	.038	0.287#	.021	0.254#	.045	0.489^	< .001

P-values < .05 were considered significant.
*Good correlation, ^Moderate correlation, #weak correlation ($r < 0.4$).

Table 3. Relation between the studied three cells and the stages of hepatic fibrosis.

	Stage of fibrosis								
	F1 ($n = 15$)		F2 ($n = 22$)		F3 ($n = 16$)		F4 ($n = 11$)		
	Mean	Standard deviation	Mean	Standard deviation	Mean	Standard deviation	Mean	Standard deviation	*P*-value
Fb	5.6^	1.9	8.8^	2.3	11.0^	3.7	10.7^	2.2	< .001
MF	16.9*	4.5	25.4*#	4.2	30.7*	4.4	33.5*#	7.6	< .001
HSC	11.6+	3.4	19.5+	5.5	19.4+	4.0	15.3	3.8	< .001

^F1 significantly different with the other three groups; $P = .009$, < .001, and < .001.
*F1 significantly different with the other three stages; $P = .008$, < .001, and < .001. #F2 significantly different than #F4, $P = .034$.
+F1 different than +F2 and +F3, $P < .001$ and < .001.

versus the quantitative mean values of myofibroblasts and HSCs, respectively. Significant correlation was detected between the stages of hepatic fibrosis and the mean values of myofibroblasts, fibroblasts, and hepatic stellate cells. This correlation was good, moderate, and weak, respectively ($r = 0.750$, $P < .001$; $r = 0.598$, $P < .001$; $r = 0.287$, $P < .021$, respectively). The quantitative values of fibroblasts and myofibroblasts in stage F4 or cirrhosis were significantly increased than stage F1 ($P < .001$ and $P < .001$, respectively). Conversely, HSCs in stage F4 fibrosis did not reveal significant increase in relation to stage F1 fibrosis (Figure 5). Significant increase was noted in the mean value of myofibroblasts and fibroblasts in severe hepatic fibrosis (F3 + F4) versus moderate fibrosis (F1 + F2) ($P < .001$; Table 4). Meanwhile HSC revealed no significant increase in severe fibrosis. The analysis of the logistic regression (Table 5) of myofibroblasts and fibroblasts pointed to the important impact of myofibroblasts on hepatic fibrogenesis versus fibroblasts. This was deduced from the *P*-value of myofibroblasts which was smaller than that of fibroblasts ($P < .001$, $P < .012$, respectively). Meanwhile, the increase in fibroblasts denoted the development of hepatic cirrhosis. Every unit increase in the mean value of fibroblasts and myofibroblasts is associated, respectively, with 41% and 30% increase in the risk of liver cirrhosis development.

Discussion

To our knowledge this is the first study which tackles the study of these three hepatic fibrogenic cells simultaneously at the level of EM and CLSM using multiple fluorochromes staining. In the present work, the quantitative assessment of α smooth muscle actin immunoreactive cells conforming with myofibroblasts, whatever its origin, revealed, respectively, moderate and good significant correlation with the corresponding morphometric image analysis of liver tissue collagen, serum levels of HA, and the stage of hepatic fibrosis. Controversially, HSCs and fibroblasts revealed weak or moderate correlation. Also, the logistic regression test has proved the significant involvement of myofibroblasts in the progress of hepatic fibrosis. These results were confirmed by EM of liver sections in which myofibroblasts and myofibroblasts transdifferentiated from activated HSCs represented the main encountered cells. These findings reinforce the published concept that myofibroblasts are the key players in the process of hepatic fibrogenesis [15,24,30,38]. Moreover, the significant correlation detected between these studied fibrogenic cells pick out the synergistic manner by which the three cells orchestrate the process of hepatic fibrogenesis. The detected myofibroblast cellular intercommunicating processes, detached

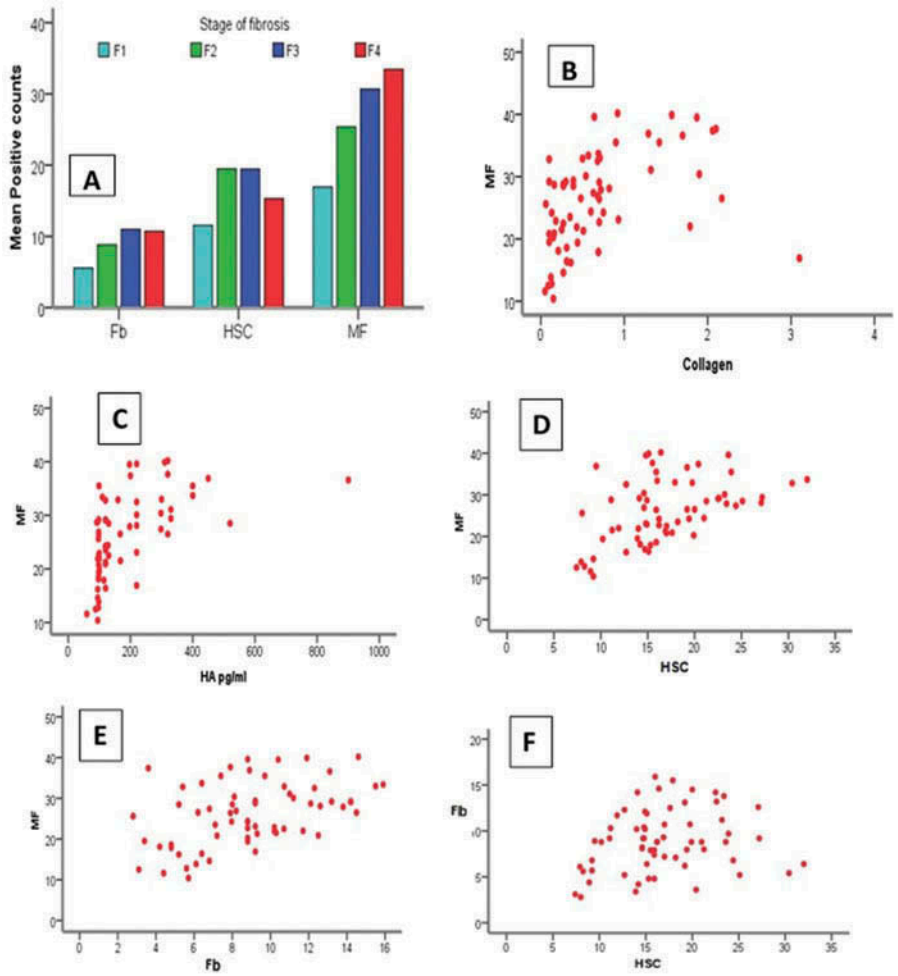

Figure 5. Figures illustrating the relations between myofibroblasts and the studied parameters. (A) The mean values of the positive cellular count of the three fibrogenic cells in relation to the stages of hepatic fibrosis. (B) Correlation between myofibroblasts and MIA of collagen. (C) Correlation between myofibroblasts and serum hyaluronic acid. (D) Correlation between myofibroblasts and HSC. (E) Correlation between myofibroblasts and fibroblasts. (F) Correlation between HSC and fibroblasts.

Table 4. Relation between moderate fibrosis (F1 + F2), severe fibrosis (F3 + F4), and the quantitative assessment of the three fibrogenic cells.

	Stage of hepatic fibrosis				
	F1 and F2 (n = 37)		F3 and F4 (n = 27)		
	Mean	Standard deviation	Mean	Standard deviation	P-value
Fb	7.5	2.6	10.9*	3.1	< .001
MF	21.9	6.0	31.8^	6.0	< .001
HSC	16.3	6.2	17.7	4.4	.288

P-values < 0.05 were considered significant. Fb significantly increased in *F3 and F4 versus F1 and F2. MF significantly increased in ^F3 and F4 versus F1 and F2.

Table 5. Logistic regression of fibroblasts and myofibroblast on the process of hepatic fibrosis.

	B	SE	Significance	Exp (B)	95% CI for EXP (B)	
					Lower	Upper
Fb	0.343	0.137	0.012	1.41	1.08	1.84
MF	0.265	0.073	<0.001	1.30	1.13	1.50
Constant	−10.733	2.618	<0.001			

B, regression coefficient; Exp B, OR or odds ratio (risk of the disease); CI, confidence intervals.

cellular spindle-shaped projections, or cleaved cellular parts, most probably carrying genetic information, may be one of the underlying contributing factors to the progress of lobular fibrosis. Also, it represents a way to maintain intercellular talk and transport of soluble mediators.

HSCs are considered by this study as well as by many other authors [11,24,30,39] as the major source of myofibroblasts. It was reported that upon activation, HSCs modify their morphology, drift to the site of injury, and differentiate into

myofibroblasts [21,39,40]. The present work add to this knowledge that myofibroblasts detected in liver lobules are mainly of HSCs origin. At the level of EM, nearly all the encountered myofibroblasts in hepatic lobules disclosed the specific morphological criteria of myofibroblast with the presence of single residual fat droplet which characterizes the myofibroblasts transdifferentiated from activated HSCs [23]. Moreover, the detected residual co-localization of reelin immunoreactivity, which is a specific marker of HSCs [28,31,41] in myofibroblasts confined in the lobular areas, confirms this observation.

For the first time, this study depicted cells showing morphological criteria of myofibroblasts, [32] distinguished from SMCs and fibroblasts, circulating in hepatic portal circulation. This finding may draw attention to the possible reliability of the transdifferentiation of myofibroblasts from bone marrow stem cells postulated by Forbes and Parola [11] rather than bone marrow–derived fibrocytes [13,39,42–44]. In this study, the recruited myofibroblasts were seen in cases of stage F4. This stage of cirrhosis was associated with decrease in the quantitative mean values of HSCs, which represent the main source of myofibroblasts. This decrease may be considered one of the triggering factors contributing to the recruitment of myofibroblasts from bone marrow.

The present work opens the door for discussing the possible modulation of myofibroblast to fibroblasts. In other words, fibroblasts represent the fate of myofibroblasts. This postulation is based on the noticed ultrastructural morphological modulation of the myofibroblast toward fibroblast configuration when trapped in area of dense collagen deposition; the detected relation between the increase in fibroblasts and the development of cirrhosis; the absence of myofibroblasts from normal liver [24,39]; the uncertainty of the reported data concerning the transdifferentiation of bone marrow fibrocytes into myofibroblasts; and the difficulty to trace the lineage of the progeny of fibrocytes in tissues [13]. All these previously reported data may support this hypothesis. In general, fibrogenic cells are not static but dynamic in nature and it is accepted that what occurs with fibroblasts and myofibroblasts in vitro or in cell culture does not closely mimic what happens in vivo [11].

In conclusion, the present work provided substantial insight on the dynamic figures of three important hepatic fibrogenic cells all through the stages of hepatic fibrosis. Also, this study proposes the possible origin of myofibroblasts from bone marrow progenitor cells and the hypothesis of its possible fate into fibroblast. This last assumption deserves further study, especially that the functional similarities and differences between myofibroblasts and fibroblasts isolated from living body are not completely identified [45].

In this context, it is recommended that parallel to the deployed effort in the production of treatment for the inactivation of HSCs [14,46–48] research targeting myofibroblast inactivation is a realistic hope for outcoming anti-fibrotic therapy.

Acknowledgments

The authors thank Prof. Dr. Inas Elattar, Professor of Biomedical Statistics at the National Cancer Institute, Egypt, for the statistical analysis of the obtained data. Thanks are due to Mr. Walid Mohamed for performing EM ultrathin sections. We acknowledge Mrs. Sahar Abbas for her assistance in the staining of liver sections using multiple immunofluorescence technique and for processing EM samples.

Author contributions: Soheir S. Mansy conceived the idea, designed and managed the study, obtained funding, organized logistics, and performed the study of liver sections at the level of light, confocal laser scanning, and electron microscopes. She analyzed and interpreted findings. She wrote the article and the discussion of the results. Mona N. Nosseir performed the morphometric image analysis. Mona A. Zoheiry carried out the assessment of serum hyaluronic acid. Moataz H. Hassanein and Mohammed F. Guda provided the study with the liver biopsies and patient clinical data. May M. Othman and Hoda A. Yehia assisted in logistics and data entry. All authors reviewed and approved the article.

Declaration of interest

The authors assert that there is no conflict of interest in regard to this article.

Funding

The authors acknowledge funding from the Science and Technology Development Fund (project number 1703).

References

1. Hajarizadeh B, Grebely J, Dore GJ. Epidemiology and natural history of HCV infection. *Nat Rev Gastroenterol Hepatol* 2013;10:553–562.

2. European Association for the study of the Liver (EASL). Clinical practice guidelines: Management of hepatitis C virus infection. *J Hepatol* 2014;60:392–420.
3. Lee YA, Wallace MC, Friedman SL. Pathobiology of liver fibrosis: A translational success story. *Gut* 2015;64:830–841.
4. Jiang JX, Török NJ. Liver injury and the activation of the hepatic myofibroblasts. *Curr Pathobiol Rep* 2013;1:215–223.
5. Schuppan D, Pinzani M. Anti-fibrotic therapy: Lost in translation? *J Hepatol* 2012;56:566–574.
6. Chen L, Li J, Zhang J, et al. S100A4 promotes liver fibrosis via activation of hepatic stellate cells. *J Hepatol* 2015;62:156–164.
7. Gressner AM, Weiskirchen R. Modern pathogenetic concepts of liver fibrosis suggest stellate cells and TCF-beta as major players and therapeutic targets. *J Cell Mol Med* 2006;10:76–99.
8. Kisseleva T, Brenner DA. Fibrogenesis of parenchymal organs. *Proc Am Thorac Soc* 2008;5:338–342.
9. Friedman SL. Hepatic stellate cells: Protean, multifunctional, and enigmatic cells of the liver. *Physiol Rev* 2008;88:125–172
10. Kisseleva T, Brenner DA. Anti-fibrogenic strategies and the regression of fibrosis. *Best Pract Res Clin Gastroenterol* 2011;25:305–317.
11. Forbes SJ, Parola M. Liver fibrogenic cells. *Best Pract Res Clin Gastroenterol* 2011;25:207–217.
12. Mederacke I, Hsu CC, Troeger JS, et al. Fate tracing reveals hepatic stellate cells as dominant contributors to liver fibrosis independent of its etiology. *Nat Commun* 2013;4:2823–2832.
13. Xu J, Min Cong M, Park TJ, et al. Contribution of bone marrow-derived fibrocytes to liver fibrosis. *Hepatobiliary Surg Nutr* 2015;4:34–47.
14. Bárcena C, Stefanovic M, Tutusaus A, et al. Gas6/Axl pathway is activated in chronic liver disease and its targeting reduces fibrosis via hepatic stellate cell inactivation. *J Hepatol* 2015;63:670–678.
15. Lei XF, Fu W, Kaneyama J, et al. Huc-5 deficiency attenuates the activation of hepatic stellate cells and liver fibrosis through upregulation of Smad7 in mice. *J Hepatol* 2016;64:110–117.
16. Miyata E, Masuya M, Yoshida S, et al. Hematopoietic origin of hepatic stellate cells in the adult liver. *Blood* 2008;111:2427–2435.
17. Goodpaster T, Legesse-Miller A, Hameed MR, et al. An immunohistochemical method for identifying fibroblasts in formalin-fixed, paraffin-embedded tissue. *J Histochem Cytochem* 2008;56:347–358.
18. Novo E, Bonzo L, Cannito S, et al. Hepatic myofibroblasts: A heterogeneous population of multifunctional cells in liver fibrogenesis. *Int J Biochem Cell Biol* 2009;41:2089–2093.
19. Atzori L, Pli G, Perr A. Hepatic stellate cell: A star cell in the liver. *Int J Biochem Cell Biol* 2009;41:1639–1642.
20. Venugopal SK, Jiang J, Kim TH, et al. Liver fibrosis causes downregulation of miRNA-150 and miRNA-194 in hepatic stellate cells, and their overexpression causes decreased stellate cell activation. *Am J Physiol Gastrointest Liver Physiol* 2010;298:G101–G106.
21. Yin C, Evason KJ, Asahina K, et al. Hepatic stellate cells in liver development, regeneration, and cancer. *J Clin Invest* 2013;123:1902–1910.
22. Nepomnyashchikh GI, Aidagulova SV, Nepomnyashchikh DL, et al. Ultrastructural and immunohistochemical study of hepatic stellate cells over the course of infectious viral fibrosis and cirrhosis of the liver. *Bull Exp Biol Med* 2006;142:723–728.
23. Mansy SS, ElKafif N, AbdelFatah A, et al. Hepatic stellate cell and fibrogenesis in cases of HCV infection: An ultrastructural insight. *Ultrastruct Pathol* 2010;34:62–67.
24. Iwaisako K, Taura K, Koyama Y, et al. Strategies to detect Hepatic myofibroblasts in liver cirrhosis of different etiologies. *Curr Pathobiol Rep* 2014;2:209–215.
25. Halfon P, Bourlière M, Pénaranda G, et al. Accuracy of hyaluronic acid level for predicting liver fibrosis stages in patients with hepatitis C. *Comp Hepatol* 2005;4:6–11.
26. Baranova A, Lal P, Birerdinc A, et al. Non-invasive markers for hepatic fibrosis. *BMC Gastroenterol* 2011;11:91–106.
27. Singer KH, Scearce RM, Tuck DT, et al. Removal of fibroblasts from human epithelial cell cultures with use of a complement fixing monoclonal antibody reactive with human fibroblasts and monocytes/macrophages. *J Invest Dermatol* 1989;92:166–170.
28. Botella-López A, Madaria E, Jover R, et al. Reelin is over-expressed in the liver and plasma of bile duct ligated rats and its levels and glycosylation are altered in plasma of humans with cirrhosis. *Int J Biochem Cell Biol* 2008;40:766–775.
29. Alt E, Yan Y, Gehmert S, et al. Fibroblasts share mesenchymal phenotypes with stem cells, but lack their differentiation and colony-forming potential. *Biol Cell* 2011;103:197–208.
30. Liu X, Xu J, Brenner DA, et al. Reversibility of liver fibrosis and inactivation of fibrogenic myofibroblasts. *Curr Pathobiol Rep* 2013;1:209–214.
31. Mansy SS, Nosseir MM, Zoheiry MA, et al. Value of reelin for assessing hepatic fibrogenesis in a group of Egyptian HCV infected patients. *Clin Chem Lab Med* 2014;52:1319–1328.
32. Schurch W, Seemayer TA, Hinz B, Gabbiani G. Myofibroblast. In: Mills SE, (ed.), *Histology for pathologists*. Philadelphia: Lippincott Williams & Wilkins, 2007, p. 125.
33. Bedossa P, Bioulac-Sage P, Callard P, et al. The French METAVIR Cooperative Study Group intraobserver and interobserver variations in liver biopsy interpretation in patients with chronic hepatitis C. *Hepatology* 1994;20:15–20.

34. Leroy V, Hilleret MN, Sturm N, et al. Prospective comparison of six non-invasive scores for the diagnosis of liver fibrosis in chronic hepatitis C. *J Hepatol* 2007;46:775–782.
35. Becker L, Salameh W, Sferruzza A, et al. Validation of Hepascore, compared with simple indices of fibrosis, in patients with chronic hepatitis C virus infection in United States. *Clin Gastroenterol Hepatol* 2009;7:696–701.
36. Ahmad W, Ijaz B, Javed FT, et al. Comparison of four fibrosis indexes in chronic HCV: Development of new fibrosis-cirrhosis index (FCI). *BMC Gastroenterol* 2011;11:44–54.
37. Johnson ID. Practical considerations in the selection and application of fluorescent probes. In: Pawley JB, (ed.), *Handbook of biological confocal microscopy*, 3rd edn. New York: Plenum Press; 2006; p. 362.
38. Seki E, Brenner DA. Recent advancement of molecular mechanisms of liver fibrosis. *J Hepatobiliary Pancreat Sci* 2015;22:512–518.
39. Iwaisako K, Brenner DA, Kisseleva T. What's new in liver fibrosis? The origin of myofibroblasts in liver fibrosis. *J Gastroenterol Hepatol* 2012;27:65–68.
40. Shirakami Y, Lee SA, Clugston RD, et al. Hepatic metabolism of retinoids and disease association. *Biochim Biophys Acta* 2012;1821:124–136.
41. Samama B, Boehm N. Reelin immunoreactivity in lymphatics and liver during development and adult life. *Anat Rec A Discov Mol Cell Evol Biol* 2005;285:595–599.
42. Abe R, Donnelly SC, Peng T, et al. Peripheral blood fibrocytes: Differentiation pathway and migration to wound sites. *J Immunol* 2001;166:7556–7562.
43. Kisseleva T, Uchinami H, Feirt N, et al. Bone marrow-derived fibrocytes participate in pathogenesis of liver fibrosis. *J Hepatol* 2006;45:429–438.
44. Scholten D, Reichart D, Paik YH, et al. Migration of fibrocytes in fibrogenic liver injury. *Am J Pathol* 2011;179:189–198.
45. Akamatsu T, Arai Y, Kosugi I, et al. Direct isolation of myofibroblasts and fibroblasts from bleomycin-injured lungs reveals their functional similarities and differences. *Fibrogenesis Tissue Repair* 2013;6:15–621.
46. Bataller R, Brenner DA. Hepatic stellate cells as a target for the treatment of liver fibrosis. *Semin Liver Dis* 2001;21:437–451.
47. Moles A, Tarrats N, Morales A, et al. Acidic sphingomyelinase controls hepatic stellate cell activation and in vivo liver fibrogenesis. *Am J Pathol* 2010;177:1214–1224.
48. Schuppan D, Kim YO. Evolving therapies for liver fibrosis. *J Clin Invest* 2013;123:1887–1901.